buildings

MDPI

Article

Molecular Dynamics Study on Interfacial Strengthening Mechanisms of Ettringite/Polymer Nanocomposites

Liwei Zhang, Heping Zheng * and Huilin Xie

Department of Civil Engineering, Qingdao University of Technology, Qingdao 266033, China; zhangliwei@qut.edu.cn (L.Z.); 17863527946@163.com (H.X.)
* Correspondence: zhengheping0802@126.com

Abstract: Compared with polymer-modified ordinary-Portland-cement-based materials, research on cement materials based on polymer-modified sulfoaluminate is still in the preliminary stage and lacks an understanding of the mechanism of the interaction interface. The aim of this work is to study the bond performance of ettringite, the main hydration product of sulfoaluminate cement, with various types of polymers using molecular dynamics methods. Steered molecular dynamics were used to simulate the separation of polyamide (PA), polyethylene glycol (PEG), polyacrylic acid (PAA) and polypropylene (PP) from ettringite substrate, reflecting the order of bond properties of the four polymers: PAA > PA > PEG > PP. The internal mechanism of bond properties between different polymers and ettringite was analyzed by studying the local structure and dynamic characteristics. The results show that a Ca–O ionic pair is formed between the calcium ions on the surface of the polymer and ettringite substrate, resulting in strong interaction. In addition, the formation of a H bond also contributes to bond performance. The properties of the polymer itself, such as the degree of polymerization and branched-chain freedom, affect the coordination of the polymer to the substrate. This study provides valuable insights for advancing the development of polymer-modified sulfoaluminate-cement-based materials.

Keywords: polymer; ettringite; interfacial bonding performance; molecular dynamics

Citation: Zhang, L.; Zheng, H.; Xie, H. Molecular Dynamics Study on Interfacial Strengthening Mechanisms of Ettringite/Polymer Nanocomposites. *Buildings* **2023**, *13*, 2976. https://doi.org/10.3390/buildings13122976

Academic Editor: Rajai Zuheir Al-Rousan

Received: 3 November 2023
Revised: 24 November 2023
Accepted: 27 November 2023
Published: 29 November 2023

1. Introduction

Portland cement has been widely used because of its reliable performance and low price. However, it also has problems, such as long maintenance time, slow development of early strength, poor fluidity and low compaction rate. Therefore, sulfoaluminate cement, which has the characteristics of fast hardening, early strength, shrinkage and short design age, has become a research focus of new building materials in recent years and is widely used in construction, roads, water conservancy, port tunnels and other fields of emergency repair. Compared with Portland cement, the CO_2 content of sulfoaluminate cement can be reduced by 40% per ton [1], which is in line with the development trend regarding low carbon emissions and high-performance cement. However, as a brittle material, cement has poor bending and tensile effects, and also has certain defects in wear resistance and flexibility, which cannot meet the requirements for its toughness and bond strength. Fortunately, polymer-reinforced cement matrix composites can solve this problem well.

Polymer materials exhibit excellent toughness and high bond strength, attributed to the relaxation movement between their chain segments. The incorporation of polymers into cement-based materials results in the formation of a polymer–cement composite system. On one hand, polymers can adsorb particles generated during cement hydration through their inherent polar functional groups, creating a network with interpenetrating structures of polymer–cement hydration products. On the other hand, the extended chain segments of polymers contribute to enhancing the stiffness of cement-based materials. This comprehensive enhancement significantly improves the toughness and bonding properties

of cement-based materials. Because polymer-reinforced cement matrix composites are still cement-based, they are more compatible with concrete substrates. Polymer-reinforced cement matrix composites have been more widely used in projects such as the Yangtze River Three Gorges Power Station, the National Theatre and municipal projects in China [2,3].

Currently, the research on polymer-modified sulfoaluminate cement is still in the preliminary stage. Scholars have carried out research on the mechanical properties, workability and toughness of polyacrylic acid and polyvinyl alcohol for sulfoaluminate-cement-based materials. The experiments have demonstrated that the incorporation of polymers effectively improves the mechanical properties of cement-based materials, and compounding could play a synergistic role to improve the flowability, increase flexural and compressive strength and enhance toughness [4–6]. Xiao et al. [7] found that the optimal dosage of polyvinyl alcohol was 0.75%, and the 28d flexural strength of mortar increased by 15% under this dosage. Zhang et al. [8] studied the effects of polyacrylamide on the setting time, mechanical properties and water resistance. The study showed that the addition of polyacrylamide could significantly prolong the setting time and improve its fluidity, among which the 3d and 28d flexural strengths increased by 75% and 39%, respectively, when the dosing amount was 0–0.3%, and the mechanical properties were greatly improved. In addition, polymers such as polyacrylic acid, polyurethane and epoxy [9–11] can improve the performance of sulfoaluminate cement very well. According to previous studies, it can be found that the macroscopic properties, such as the mechanics of polymer-reinforced cement matrix composites, are mainly studied, while the study of the interfacial interaction between the two phases at the nanoscale is still imperfect and challenging, occurring only through experimental studies, where molecular dynamics has a significant advantage [12,13].

Molecular dynamics (MD) simulation can break the limitations of time and conditions, demonstrate experimental laws at the atomic level, realize the exploration of mechanisms and can also combine with the experimental development of novel materials [13,14]. Molecular dynamics has been used to elaborate and reveal the integrated interfacial mechanism between polymers and hydrated calcium silicate (C–S–H) [15]. Wang et al. [16] revealed the reasons for the differences in interfacial shear strength between different polymer fibers and C–S–H by the molecular dynamics method. Hou et al. [17] proved that the interfacial bonding between C–S–H and polymers is related to the polarity of polymer functional groups, H bonds, Ca–O ionic pairs and bond stability. Liu et al. [18] found that electrostatic and H-bond interactions increased the adhesion properties of cellulose fiber to the C–S–H interface. Zhou et al. [19,20] investigated the interaction mechanism of PVA with the micro-test method and MD simulations. However, there are significant differences in the composition of ordinary Portland cement and sulfoaluminate cement. The strength of ordinary-Portland-cement-based material is derived from the interaction between C–S–H gels, while the strength of sulfoaluminate-cement-based material is derived from ettringite crystals, which account for about 65% of the hydration products. Therefore, there may be differences in the affinity and bonding properties of the polymers to the two types of cement.

Due to the lack of targeted studies on the bonding performance of polymers with an ettringite interface, in this work, the bond performance of ettringite, the main hydration product of sulfoaluminate cement, with four types of polymers was investigated via the molecular dynamics method for the first time. The tensile strength of the four polymers separated from the ettringite substrate was simulated separately by tensile dynamics to reflect the bonding performance between the four polymers and ettringite. The intrinsic mechanism of bonding performance between different polymers and ettringite was analyzed by local structural and dynamic characterization. This work is instructive for the development of polymer-modified sulfoaluminate-cement-based materials.

2. Simulation Method

2.1. Model Construction

The initial model for the study is based on existing modeling of ettringite utilizing crystals from a crystal library [21]. Ettringite, with the molecular formula $3CaO{\cdot}Al_2O_3{\cdot}3CaSO_4{\cdot}32H_2O$ and a basic structural unit of $[Ca_3Al(OH)_6{\cdot}12H_2O]^{3+}$, exhibits a columnar structure depicted in Figure 1a [22–24]. These columns consist of lines of $[AI(OH)_6]^{3-}$ octahedra along the (001) direction, connected to neighboring columns by three groups of Ca^{2+} ions, completing coordination polyhedra with water molecules. Each Ca^{2+} ion is 8, coordinated by 4 H_2O molecules and 4 OH^- ions, forming a trigonal prism. The polyhedra share edges with adjacent $[AI(OH)_6]^{3-}$ octahedra. $SO_4{}^{2-}$ ions and remaining water molecules are hexagonally arranged in the cylindrical gap, encircling the positively charged cylinder's axis.

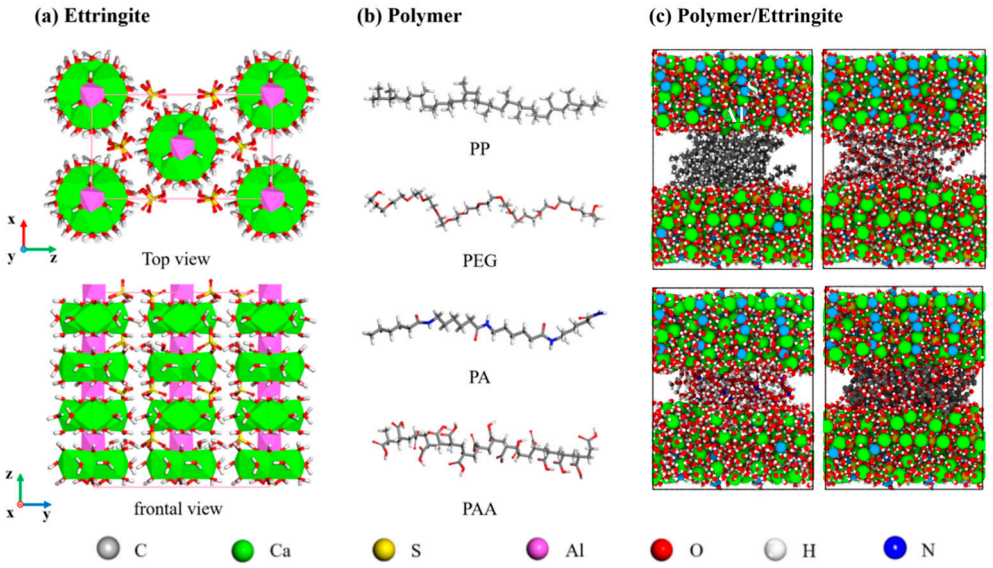

Figure 1. (**a**) Crystal structure model of ettringite; (**b**) four polymer models; (**c**) composite structure model.

Secondly, four representative polymers with different functional group types are selected, which are non-polar polypropylene as the control, polyethylene glycol with hydroxyl functional group, polyamide with amide functional group and polyacrylic acid with carboxyl functional group. Under the condition of the same number of functional groups, the molecular model is established by selecting the degree of polymerization of polypropylene polyethylene glycol and polyacrylic acid as 16. Due to the large molecular formula of polyamide monomer, on the premise that the main chain length of polyacrylic acid is basically the same as that of the other three polymers, the degree of polymerization is four. Their molecular structure formula is shown in Figure 1b.

The ettringite model of the bottom and top layers is created by means of the super cell, and the parameters are as follows: a = 44.67 Å, b = 38.68 Å, c = 25.87 Å. The polymer is left in 25 Å space between the two parts of ettringite. The four polymer molecules are placed in the middle of the ettringite in two layers of four for each layer to form the composite structural model of the sandwich. In addition, a vacuum layer of 80 Å is reserved at the top to prevent ettringite from crossing periodic boundaries and causing interaction between upper and lower layers, and the simulation box is large enough to accommodate the bonding and stripping behavior of ettringite and polymer. The balanced structures of the four materials are shown in Figure 1c.

2.2. Simulation Details

In this study, the ClayFF [25] force field is employed to characterize the interactions within ettringite substrates, offering a detailed representation of their structural dynamics.

Simultaneously, the CVFF force field is harnessed to delineate the interactions occurring within polymers [26]. The ClayFF has been proved to accurately describe the interaction of clay hydroxide and interface structure and has also been successfully applied in the molecular dynamics study of the interaction between cement-based materials. Ettringite is one of the hydration products of cement-based materials. The ClayFF force field does not provide for sulfate interactions, so sulfate parameters from Cannon [27,28] are used as supplements, with sulfur charges of 2e and oxygen charges of −1e. The non-bond interaction parameters and the charges of each atom in ettringite are referenced from Ref. [25]. The comprehensive simulation, executed using Lammps [29], incorporates the efficient descent method to systematically relax the entire system, aiming to minimize overall energy. Following system relaxation, an equilibrium adsorption phase is conducted under the NVT ensemble for a duration of 3 nanoseconds. To facilitate subsequent microstructure analysis, trajectory data are output at regular intervals of 1 picosecond (lps) throughout the simulation period. This meticulous approach ensures a thorough exploration of system dynamics, allowing for in-depth examination and interpretation of the resulting microstructural features.

At the stage of steered molecular dynamics, in the NVT system [30–32], an external force of the form shown below is applied to the centroid portion of the upper ettringite:

$$F = K((X_0 + V \times t) - X_{com})$$

where F is external force; K is the spring force constant, set as 0.0005 kcal/mol/nm^2; X_0 is the initial Z coordinate of the selected upper ettringite core [33]. V is the pulling speed of the reference point along the Z axis, set as 100 m/s. T is the simulation time; X_{com} is the selected dynamic location of the upper ettringite core along the Z direction. The schematic diagram of the polymer and ettringite matrix model under the action of additional forces is shown in Figure 2. To guarantee the precision of the tensile process simulation, a meticulous approach is adopted. The simulation step is finely tuned to 0.1 femtoseconds, and the simulation time is extended to 20 nanoseconds. This meticulous setup aims to capture the intricate details of the dynamic tensile behavior. Throughout the simulation process, data for force (F) and the center of mass displacement (X_{com}) are meticulously extracted. This extraction process enables the derivation of a comprehensive tensile force–displacement curve. By employing these finely tuned parameters and extracting key data points, the simulation aims to provide a detailed and accurate representation of the tensile behavior, facilitating a thorough analysis of the material's response under tensile loading conditions. In this study, Visual Molecular Dynamics (VMD) is utilized for graphical visualization [34].

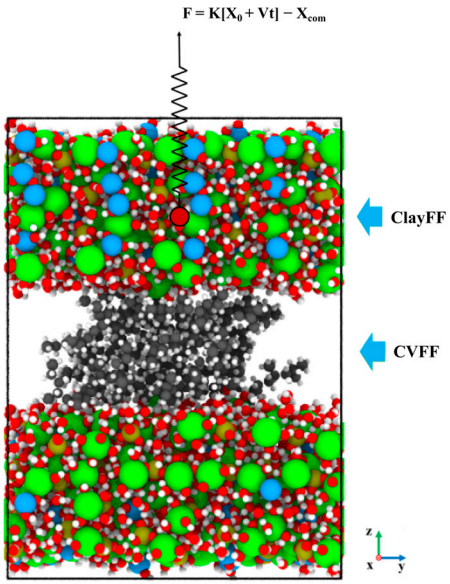

Figure 2. The steered molecular dynamics models of PA/ettringite.

3. Results and Discussion

The pulling force of the separation of the four polymers and ettringite substrate is simulated by steered molecular dynamics to reflect the interfacial bond property between the four polymers and ettringite. The microscopic mechanism of the difference in interfacial bonding properties is analyzed by local structural and dynamic characterization.

3.1. Separation Behavior

In order to preliminarily observe the behavior changes of four polymers, we extract the behavior change images of ettringite and four polymers during tensile dynamics. Simulation snapshots of the four systems are shown in Figure 3, which intuitively reflect the adsorption and separation behavior of the polymers.

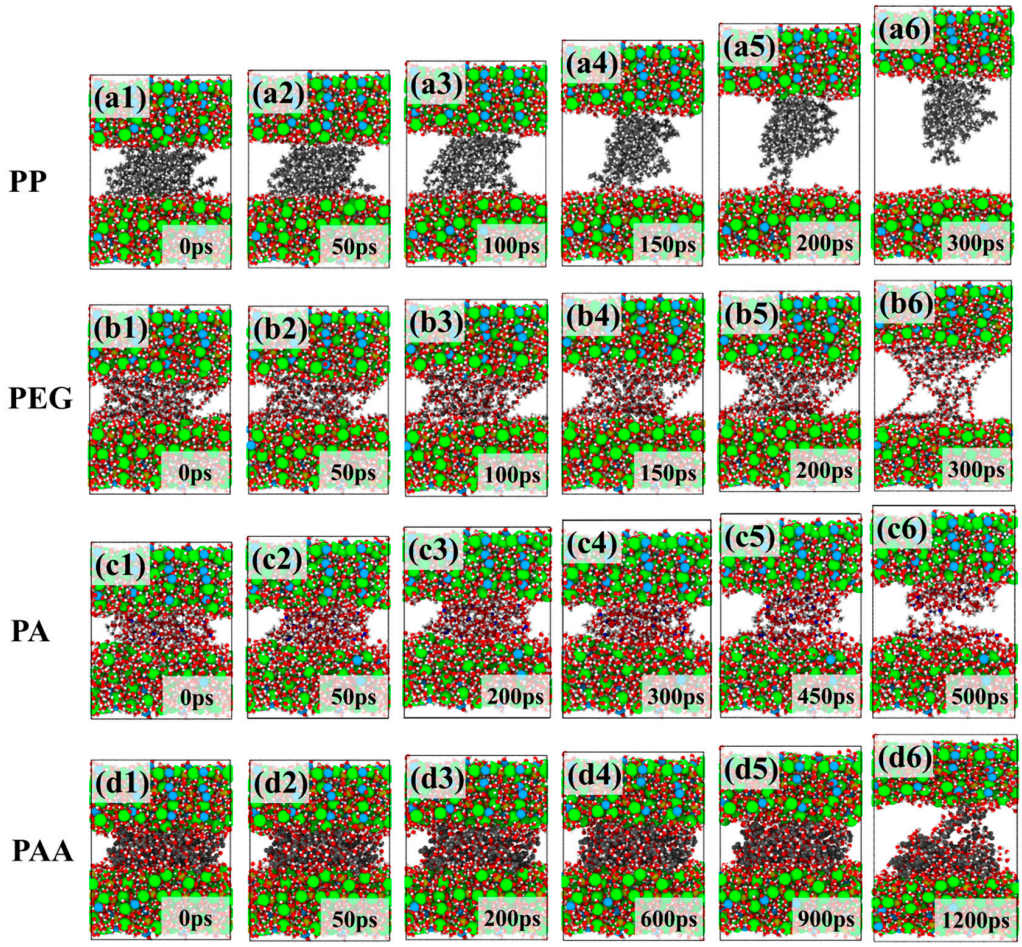

Figure 3. (**a1**–**a6**), (**b1**–**b6**), (**c1**–**c6**), and (**d1**–**d6**) indicate the damage snapshots of Ettringite/PP, Ettringite/PEG, Ettringite/PA, and Ettringite/PAA at different times, respectively.

The image comparison shows that the interface region between the four polymers and ettringite is separated with the increase in stretching time. PP is the first to detach, followed by PEG, PA and PAA. The bond strength relationship between the four polymers and ettringite can be qualitatively reflected from the simulated snapshots as PAA > PA > PEG > PP.

3.2. Force–Displacement Curves

Based on the qualitative analysis in the preceding section, the mechanical curve is extracted for quantitative analysis. Figure 4 shows the tensile force–displacement curves of the four polymers at a simulated tensile speed of 100 m/s using the tensile dynamics method. The slope of a curve is the ratio of the stretching force to the displacement at the

stretching point. When the tensile force does not reach the critical value of the interfacial force, the value is positive. When the tensile force reaches the maximum value, that is, after the polymer is separated from the ettringite base, the slope becomes negative and remains unchanged.

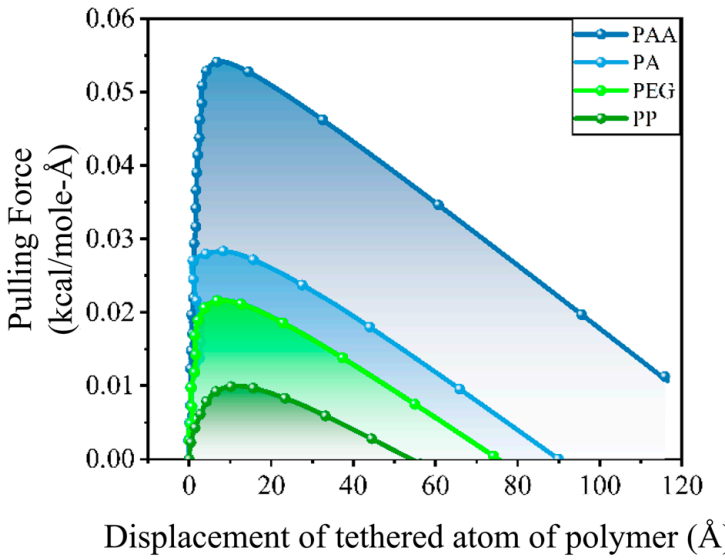

Figure 4. The ratio of the pulling force of the four polymers to the displacement.

It can be found from the curve of tensile dynamics simulation that the interface bond properties of four polymers and ettringite from high to low at the same tensile speed of different polymers are as follows: PAA > PA > PEG > PP. The first half of the curve is wavy because the chemical bond between the polymer and ettringite base is not completely disconnected in the tensile process, and the phenomenon of reconnection occurs.

The above laws are in good agreement with the experiment. Bezerra et al. [6,35] studied PVA and PP, both enols, and showed that the strength and toughness of PVA were higher than those of PP, and PVA had better adhesion to the substrate. At present, there are experimental studies on the properties of the four types of polymers modified, but there is a lack of horizontal comparison of the four polymers. Therefore, this work can effectively guide the selection of polymers and the development of experiments from the perspective of simulation. In the following sections, the mechanisms behind the differences in bonding performance between various polymers and ettringite were analyzed by the local structural and dynamic characteristics.

3.3. Atomic Intensity Distribution

The atomic intensity distribution can reflect atoms of the polymer on the surface of the ettringite. Figure 5a–d describe the intensity distribution of polyamide, polyacrylic acid, polyethylene glycol and the components between the four polymers, respectively, where Ca denotes the ettringite surface calcium atom, Os denotes the polymer single-bond oxygen atom, Od denotes the polymer double-bond oxygen atom, Oco denotes the polymer carboxyl oxygen atom, Oc denotes the polymer main-chain oxygen atom, Hal denotes the aluminum hydroxyl group of ettringite and C denotes the polymer main-chain carbon atom. While ensuring the same length of the main chains of the four polymers, the atomic content of the main chains of the polymers differed due to the degree of polymerization, so we mainly observe the changes in the intensity distribution of each polymer atom in terms of position.

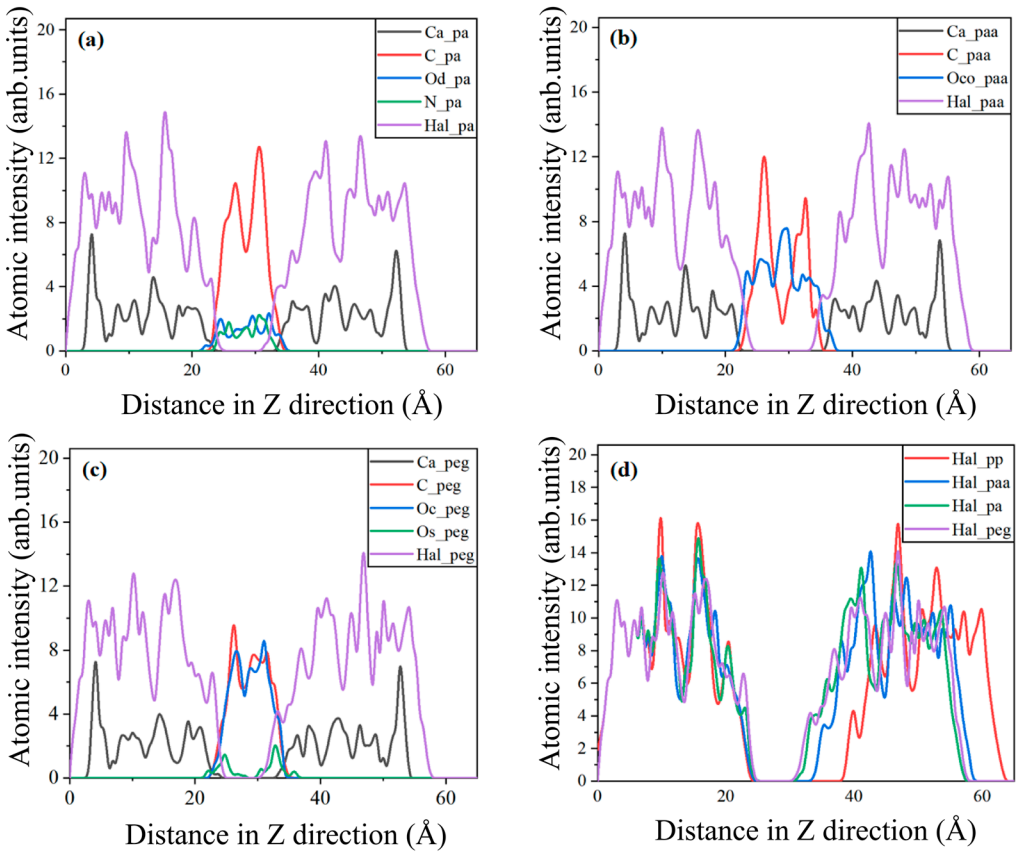

Figure 5. Atomic intensity distribution of different composite material systems: (**a**) Ettringite/PA, (**b**) Ettringite/PAA, (**c**) Ettringite/PEG, (**d**) Hydrogen atoms in four polymers.

It can be seen from Figure 5a that the Od intensity distribution is closer to the Ca layer than its main-chain carbon atoms at the ettringite interface, indicating the strong interaction between calcium atoms near the interface between polyamide and ettringite, which causes its distribution to shift. The atomic strength distribution of polyacrylic acid and ettringite substrate is shown in Figure 5b. The intensity peak of Oco of the carboxyl functional group of PAA is close to that of Ca, and, from the overall view of the polymer, the carboxyl Oco is biased to be distributed on the side of the main-chain C close to the substrate. Both phenomena can reflect the interaction of PAA with Ca of the surface layer of ettringite. Different from the former two kinds of polymers, polyethylene glycol is out of the side chain of hydroxyl functional groups, and the main chain also exists in the more electronegative Oc. From Figure 5c, the intensity distribution can be observed; the intensity peak of hydroxyl Os is very close to the intensity peak of Ca, both with strong interaction, while the main-chain oxygen, due to the restrictions of the main chain itself, does not show a bias towards the base. In addition to the interaction mentioned above, it can be obviously found from Figure 5d that Hal of the ettringite substrate of the PAA, PA and PEG system is more inclined to the intermediate polymer layer than the PP system, indicating that there is H-bond interaction between the three polymers and the substrate. The specific bonding situation will be analyzed later.

Fundamentally, due to the polarity of the polymer itself, the above three polymers interact with the surface calcium and hydroxyl groups of the ettringite substrate, reflecting the adsorption characteristics of the polymer and the substrate.

3.4. Local Interface Analysis

In order to accurately analyze the bond situation at the interface between polymer and ettringite, and exclude the influence brought by the complexity and diversity of the intermediate polymer layer, a single polymer at the interface was selected for subsequent analysis.

3.4.1. Interfacial Ca–O Ionic Pair

The radial distribution function (RDF) can qualitatively reflect the interface structure of polymers and ettringite [36]. Figure 6a–d show the bonding of the three polymer functional groups, PAA, PA and PEG, to the surface calcium of ettringite. In the PA/ettringite interface, the first peak of Ca–Od is 2.55 Å, which is consistent with the bond length of the calcium–oxygen polyhedron in ettringite crystal between 2.35 and 2.75 Å [37]. Therefore, the sharp peak of PA indicates that the double-bonded oxygen on the amide group is bonding with the surface Ca, and the peak value is high, indicating the strong interaction between the two. Figure 6e is a partial schematic diagram of the Ca–O ionic pair of PA and ettringite, which intuitively shows the bonding situation of the interface. This simulation phenomenon is consistent with the experimental characterization of the polymer in the process of cement modification and will participate in the chemical reaction regarding the formation of the Ca–O ionic pair [11,38,39].

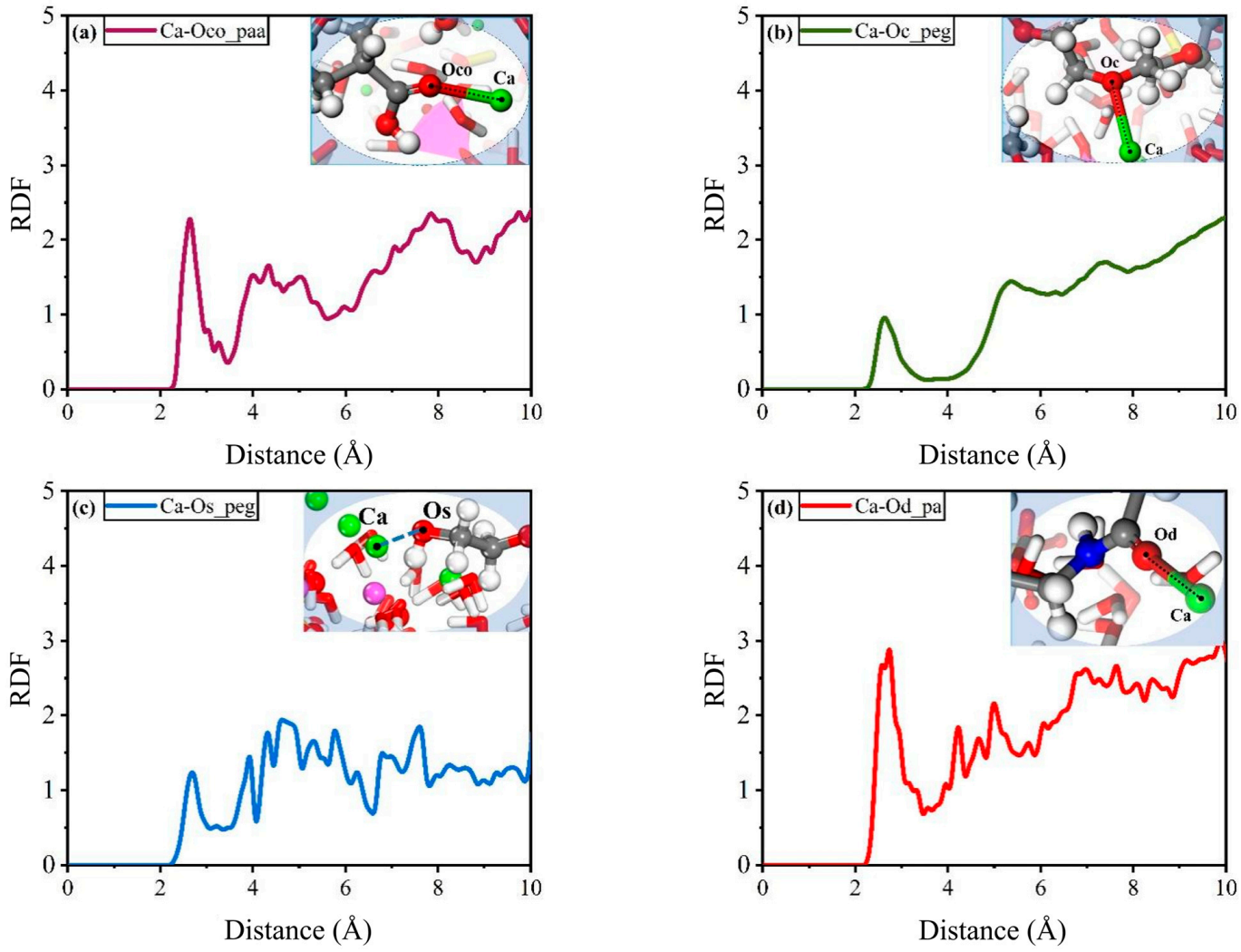

Figure 6. *Cont.*

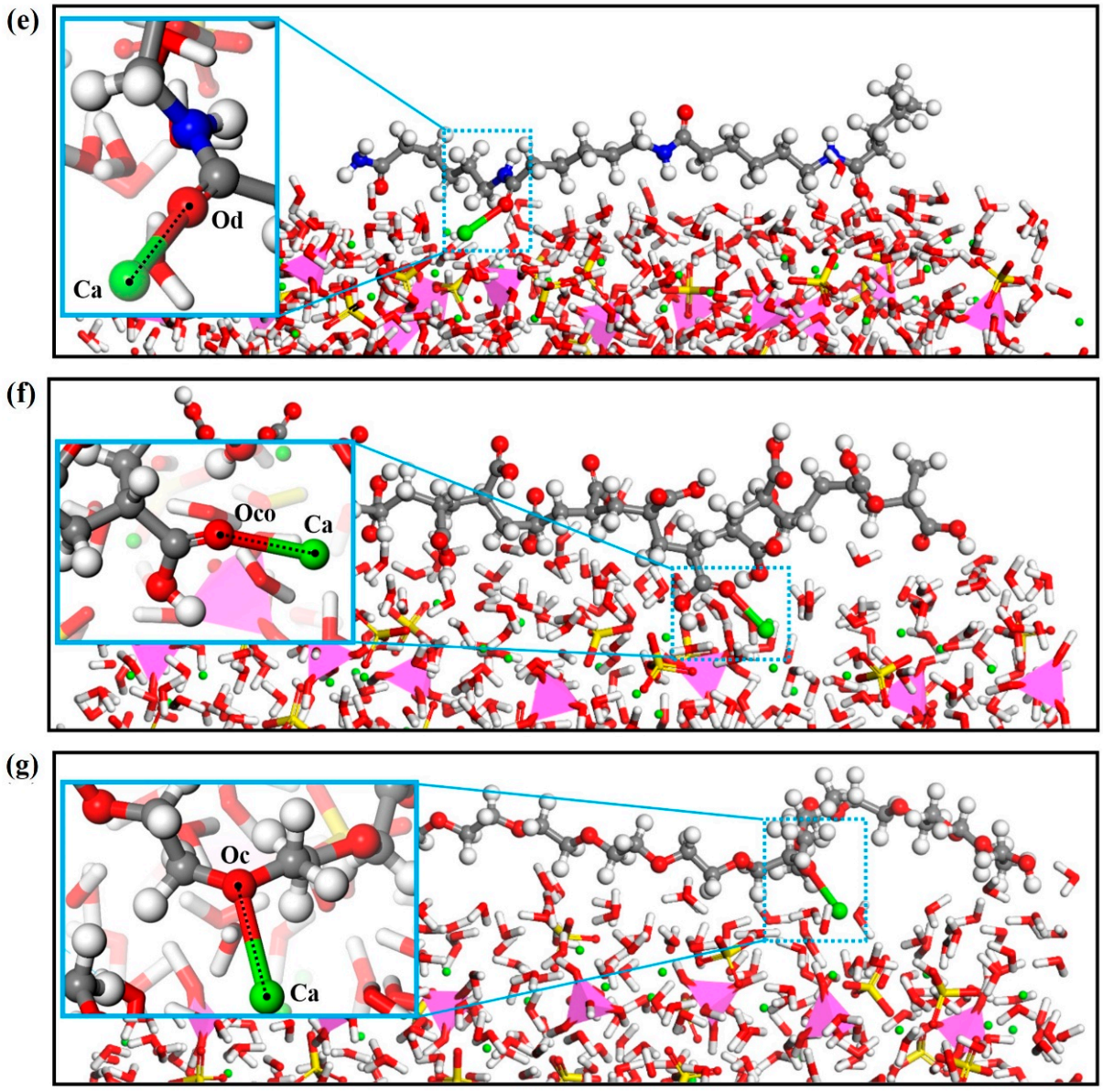

Figure 6. (**a**–**d**) The RDF of Ca–O; (**e**) local schematic diagram of Ca–O ionic pair at PA/ettringite interface; (**f**) local schematic diagram of Ca–O ionic pair at PAA/ettringite interface; (**g**) local schematic diagram of Ca–O ionic pair at PEG/ettringite interface. The blue box shows a partial enlargement of the chemical bond.

Similarly, the first peak of Ca on the surface of PAA and ettringite is about 2.65 Å, indicating that oxygen atoms of the carboxyl group in PAA can interact with calcium atoms on the ettringite interface. In PEG/ettringite composites, the first peaks of Ca–Os and Ca–Oc are both at 2.65 Å, respectively, indicating that the surface Ca of ettringite interacts not only with the hydroxyl group at the end of the PEG chain but also with the oxygen atom on the PEG main chain. This analysis method is consistent with the related simulation studies on polymers and CSH, indicating that polymer functional groups can interact with the substrate to achieve performance improvement [15,16,40,41]. The bonding between PAA, PEG and the ettringite interface is shown in Figure 6f,g.

The coordination number can be used to quantitatively analyze the interaction between different polymers and ettringite [36]. Table 1 shows the number of coordination calcium atoms of each polymer. The three polar polymers can coordinate with the surface calcium of ettringite, and the overall order of the total coordination number of the three polymers

is PAA > PA > PEG. The coordination number of PAA is three times that of PA and PEG, indicating that PAA has the stronger binding ability with ettringite surface, mainly because the carboxyl molecular structure of the PAA branch chain is larger and the degree of freedom is higher, which makes it easier to capture the surface calcium of ettringite.

Table 1. The coordination number of calcium ions between each polymer and ettringite substrate.

CN	Ettringite/PA	Ettringite/PAA	Ettringite/PEG
Ca–Od	1.30	/	/
Ca–Os	/	/	0.58
Ca–Oco	/	4.38	/
Ca–Oc	/	/	0.66
Total	1.30	4.38	1.24

While ensuring that the main chain length of all kinds of polymers is basically the same, the degree of polymerization of PA is only one-fourth that of other polymers, and the number of functional groups is significantly smaller; thus, its value on the number of coordination calcium atoms is relatively small. In addition, the number of oxygen atoms in the main chain of PEG is much larger than that of hydroxyl oxygen at the end of the chain, but there is little difference between them in the coordination number, indicating that the main-chain oxygen atoms are difficult to bind to the calcium ions due to the limitation in the degree of freedom, and calcium prefers to adsorb on the hydroxyl oxygen. Thus, it can be seen that the polymerization degree, branched chain degrees of freedom and other properties of the polymer will affect the coordination of the polymer to the substrate.

3.4.2. H Bond

Apart from the crucial Ca–O ionic pair, the interaction between ettringite and the polymer involves H bonds that significantly influence the overall bond performance at the interface. In Figure 7, the Radial Distribution Function (RDF) diagram and local structure diagram elucidate the H-bond interactions between the polymer and ettringite. Here, H represents the hydrogen in the polymer functional group, Ow denotes water oxygen, Os signifies sulfate oxygen and Oal represents the oxygen in the aluminum hydroxyl group. The ettringite surface, comprising water molecules, aluminum hydroxyl groups and sulfate, facilitates the formation of two types of H bonds with the polymer. One type involves the oxygen atom as the acceptor, capable of accepting electrons from the hydrogen atom in the polymer functional group. The other type features the hydrogen atom as the donor, providing electrons to the oxygen atom of the polymer functional group. This dual role of H bonding underscores the intricate nature of the interactions at the polymer–ettringite interface, emphasizing the diverse mechanisms contributing to the overall bond performance. The detailed analysis presented in the RDF and local structure diagram enhances our understanding of the complex intermolecular dynamics governing the interface.

Figure 7a is the RDF curve of the PAA system. It can be seen from the figure that PAA can form five types of H bonds with the base within the bond formation range of 2.45 Å, and the H bonds formed are mainly with oxygen atoms of sulfate and oxygen atoms in water. The local structure diagrams of five kinds of bonds are shown in the blue box in Figure 7b. The peak position of the RDF diagram shows that only two representative polymers are indicated to show the H bond between the polymer and ettringite substrate more intuitively and briefly. Figure 7b shows the distribution of H bonds of all PAAs. It can be found that H bonds can also be formed among PAA, which increases the bond between polymers and increases the bond strength between PAA and the ettringite interface. In Figure 7c for the RDF curves of the PA system, PA is special in that the H-bond receptor comes from the amino nitrogen atoms, has less electronegativity than O atoms and, coupled with the number of functional groups, was only about a quarter of the PAA, decreasing the likelihood to form H bonds, so the hydrogen atoms form a H bond on the functional

groups of the aft peak position, and the peak fell. The basket on the right of Figure 7d is the local diagram of H bonds. Similarly, there are H bonds between PA chains. It can be seen intuitively that the number of H bonds in PA decreases due to the small number of functional groups.

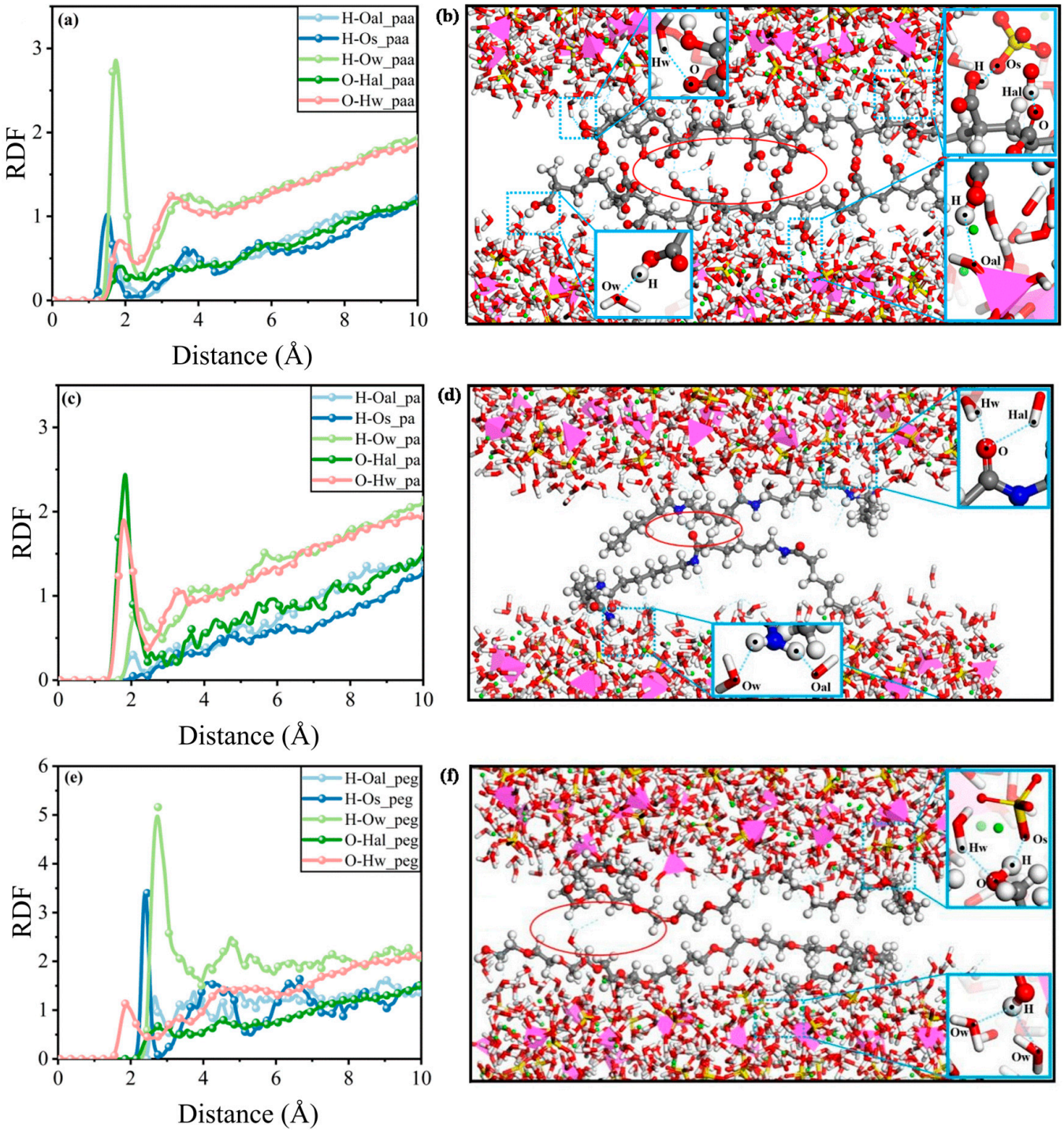

Figure 7. (**a**,**c**,**e**) represent RDF graphs of hydrogen bonds between Ettringite and PAA, PA and PEG, respectively. (**b**,**d**,**f**) represent the structure diagram of hydrogen bonds between Ettringite and PAA, PA and PEG, respectively.The inside of the red circle represents the hydrogen bond between the polymers. The inside of the blue circle represents the hydrogen bond between the polymer and the ettringite.

The H-bond RDF curve of PEG is shown in Figure 7e. It can be seen from the curve that PEG mainly forms H bonds with water molecules and sulfate, while the H bond with the aluminum hydroxyl group is weak, and its bond is shown in the blue box in Figure 7f. By comparing the left of Figure 7b,d,f, it can be found that the H-bond relationship between molecules is PAA > PA > PEG, and the intermolecular interaction of polymers enhances the interfacial bonding properties between polymers and ettringite substrate.

3.4.3. Time Correlation Function

The bond formation and coordination number of different polymers and ettringite substrates were analyzed in the previous section, and bond stability also determines the strength of bond performance. The time correlation function (TCF) can be used to describe the stability of chemical bonds between different ions; the faster the TCF curve decays with time, the weaker the bond connection [42]. Figure 8a is the time correlation function of the Ca–O ionic pair. It can be seen from the figure that the TCF value of the Ca–O ionic pair of PAA is maintained at about 0.9, and the stability is the best. The two Ca–O ionic pairs of PEG exhibit different stability, and the bonding stability of oxygen atoms in the main chain is higher than that of the terminal hydroxyl group. It can be shown that the main-chain oxygen atom is the main source of PEG forming the Ca–O ionic pair. The Ca–O ionic pair stability of PA is between PAA and PEG. In analyzing the stability order of the Ca–O ionic pair among three polymers—PAA, PA and PEG—it is evident that PAA exhibits the highest stability, followed by PA and PEG. This order aligns consistently with prior examinations of bond formation. The intricate interplay of chemical structures within each polymer contributes to the observed variations in Ca–O ionic pair stability. The preference for PAA suggests specific molecular features enhancing its bond strength, reinforcing the importance of understanding polymer characteristics in the context of bond dynamics. The established order sheds light on the nuanced relationships between polymer composition and the strength of Ca–O ionic pairs, offering valuable insights for applications in various scientific and industrial domains reliant on these materials.

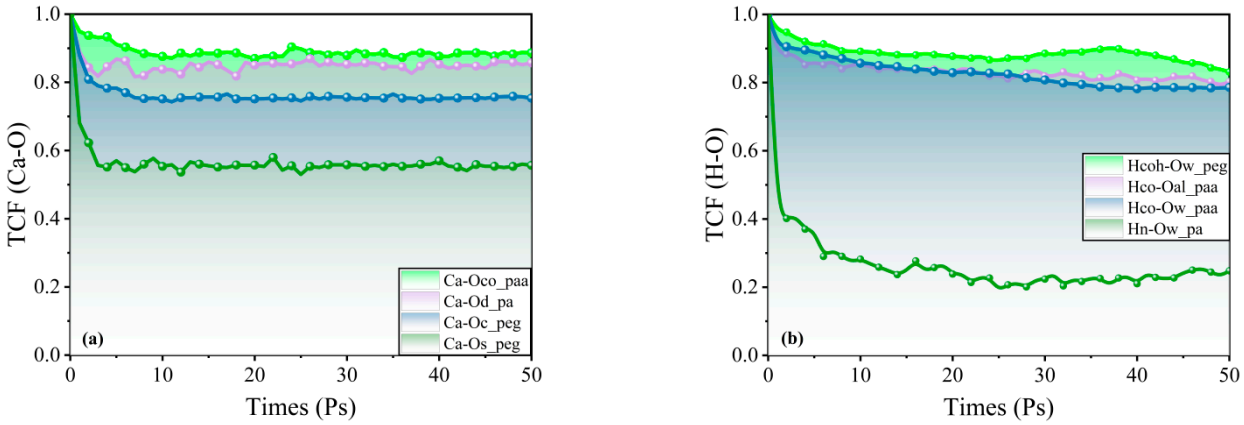

Figure 8. Time correlation function of ettringite and PAA, PA, PEG connection: (**a**) Ca–O, (**b**) H bond.

Figure 8b shows the stability of the H bond. The stability of the H bond formed by the amino group of PEG and ettringite is relatively poor, and the TCF value is about 0.25. For PAA and PA, although the above local structure analysis results show that the number of H bonds formed is small, its stability is high, which is inseparable from the fact that there are more water layers on the surface of the ettringite substrate. The H bond between polymer and substrate is still an important source of interfacial bond performance.

3.5. Dynamic Coordination Number

According to the above microscopic analysis of local structure, the bond performance between polymer and ettringite interface mainly depends on the interaction of Ca–O ionic

pair strength and H-bond interaction. In order to quantitatively characterize the changes in the interface during the tensile process, the changes in coordination number over time, i.e., dynamic coordination numbers, of the two bonds were statistically analyzed, as shown in Figure 9. As can be seen from Figure 9a in the Ca–O dynamic coordination map, the curve shows a trend of rising first and is then stable in the first 300 ps, which is consistent with the equilibrium stage of polymer and substrate in the first 300 ps, where the two interact and the coordination number increases first and then achieves stable adsorption. At the stretching stage of 300 ps, the coordination number showed a downward trend. At a1, a2 and a3, the coordination number of the corresponding polymer decreased sharply and then remained stable. Combined with Figure 3, it can be found that this turning point corresponds to the time when the polymer separates from the substrate, which can reverse-prove that the three polymers bond with the substrate through Ca–O ionic pairing. In addition, the coordination number relationship of the three polymers can also be the strength of the bond: PAA > PA > PEG. Similarly, the dynamic coordination number of H bonds (Figure 9b) also shows a corresponding sharp decrease and stable stage at the time of polymer separation, b1 and b2, respectively, but peg does not change significantly due to the small number of H bonds, which is consistent with the previous analysis. The H bond is not the main source of PEG bond performance.

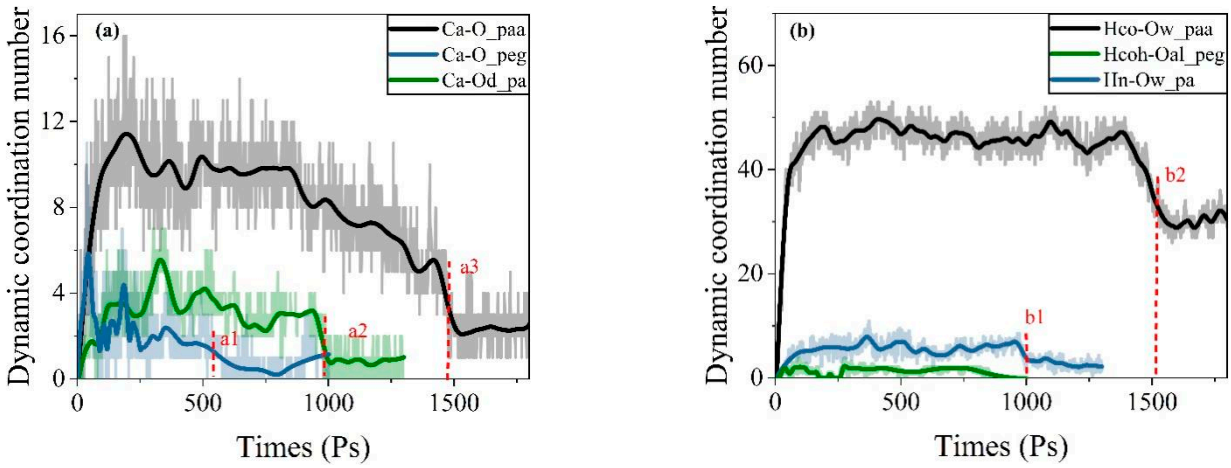

Figure 9. Dynamic coordination number: (**a**) Ca–O, (**b**) H bond. a1, a2, and a3 represent the coordination number of Ca–O bonds at 500 ps, 1000 ps, and 1500 ps respectively. b1 and b2 represent the coordination number of hydrogen bonds at 1000 ps and 1500 ps, respectively.

4. Conclusions

In this work, the interfacial bonding properties between ettringite and polymers were investigated by molecular dynamics for the first time. The separation process of four polymers, PA, PAA, PEG and PP, from ettringite was simulated by steered molecular dynamics to characterize the strength of the interfacial bonding properties of the four polymers, and the microscopic mechanisms of the differences in interfacial bonding properties were analyzed by local structural and dynamic characterization. The main findings of this work are as follows:

1. Under the tensile dynamics simulation adopted in this paper, the order of tension required for the separation of the four polymers from the interface bond is PAA > PA > PEG > PP. In the interaction with polar ettringite substrate, three polar polymers show better bonding properties than non-polar PP, and the types of polar functional groups in the polymer have a key influence on the strength of the interaction.
2. Through the microscopic mechanism analysis of local structure, it is found that the polymer can form a Ca–O ionic pair with ettringite surface calcium atoms, resulting in a strong interaction. Oxygen atoms on PA, PAA and PEG non-backbone chains can provide sites to bind calcium ions, and oxygen atoms on the PEG backbone

chain can also provide sites for calcium atoms, but, due to limitations in freedom, the coordination number value is relatively small.

3. In addition to the Ca–O ionic pair, the H bond between ettringite and polymer also determines the bond performance of the interface. The carboxyl group of PAA, the amino group of PA and the hydroxyl group of PEG provide sites for the formation of H bonds.

This study unveils the molecular-scale interface bond mechanism between ettringite and polymers, providing valuable insights into characterizing the bond properties of four types of polymers on ettringite surface. These findings offer guidance for advancing polymer-modified sulfoaluminate-cement-based materials.

Author Contributions: Methodology, H.Z.; Investigation, L.Z., H.Z. and H.X.; Writing—original draft, L.Z. All authors have read and agreed to the published version of the manuscript.

Funding: This research received no external funding.

Data Availability Statement: Data are contained within the article.

Conflicts of Interest: The authors declare no conflict of interest.

References

1. Taylor, M.; Tam, C.; Gielen, D. Energy efficiency and CO_2 emissions from the global cement industry. *Korea* **2006**, *50*, 61–67.
2. Sakai, E.; Sugita, J. Composite mechanism of polymer modified cement. *Cem. Concr. Res.* **1995**, *25*, 127–135. [CrossRef]
3. Wang, R.; Li, J.; Zhang, T.; Czarnecki, L. Chemical interaction between polymer and cement in polymer-cement concrete. *Bull. Pol. Acad. Sciences. Tech. Sci.* **2016**, *64*, 785–792. [CrossRef]
4. Song, S.H.; Liu, F.T.; Huang, Y.B. Effect of Polymer Latex and Fiber on Properties of Sulpho Aluminate Cement Mortar. *Adv. Mater. Res. Trans. Tech. Publ.* **2012**, *450*, 402–406. [CrossRef]
5. Nematzadeh, M.; Dashti, J.; Ganjavi, B. Optimizing compressive behavior of concrete containing fine recycled refractory brick aggregate together with calcium aluminate cement and polyvinyl alcohol fibers exposed to acidic environment. *Constr. Build. Mater.* **2018**, *164*, 837–849. [CrossRef]
6. Zhang, C.; Liu, Y.; Zhang, M. PP/PVA Fiber Reinforced Sulphoaluminate Cement-Based Rapid Repair Material. *Bull. Chin. Ceram. Soc.* **2021**, *40*, 2174–2183. [CrossRef]
7. Xue-jun, X.; Yu, L.; Yu-fei, J. Experimrntal Study on Mechanical Performances of Fiber Reinforced Repair. *China Concr. Cem. Prod.* **2018**, *12*, 49–52. [CrossRef]
8. Zhang, H.; Zhou, R.; Liu, S.; Zhu, Y.; Wang, S.; Wang, J.; Guan, X. Enhanced toughness of ultra-fine sulphoaluminate cement-based hybrid grouting materials by incorporating in-situ polymerization of acrylamide. *Constr. Build. Mater.* **2021**, *292*, 123421. [CrossRef]
9. Tian, Y.; Li, Z.J.; Ma, H.Y.; Jin, X.Y.; Jin, N.G. Physical and chemical influence of polyacrylate latex on cement mortars. *Adv. Mater. Res. Trans. Tech. Publ.* **2011**, *261*, 807–811. [CrossRef]
10. Liu, H.; Zhao, P.; Lu, L.; Wang, S.; Chen, M.; Cheng, X. Effect of Composition on Waterproofing Property of Silicone Modified Polyacrylate Emulsion-Sulphoaluminate Cement Composite Coating: Optimization by Response Surface Methodology. *J. Inorg. Organomet. Polym. Mater.* **2019**, *29*, 429–435. [CrossRef]
11. Wang, M.; Wang, R.; Zheng, S.; Farhan, S.; Yao, H.; Jiang, H. Research on the chemical mechanism in the polyacrylate latex modified cement system. *Cem. Concr. Res.* **2015**, *76*, 62–69. [CrossRef]
12. Rapaport, D.C.; Rapaport, D.C.R. *The Art of Molecular Dynamics Simulation*; Cambridge University Press: Cambridge, UK, 2004.
13. Alder, B.J.; Wainwright, T.E. Studies in molecular dynamics. I. General method. *J. Chem. Phys.* **1959**, *31*, 459–466. [CrossRef]
14. Hansson, T.; Oostenbrink, C.; van Gunsteren, W. Molecular dynamics simulations. *Curr. Opin. Struct. Biol.* **2002**, *12*, 190–196. [CrossRef] [PubMed]
15. Hou, D.; Yu, J.; Wang, P. Molecular dynamics modeling of the structure, dynamics, energetics and mechanical properties of cement-polymer nanocomposite. *Compos. Part B Eng.* **2019**, *162*, 433–444. [CrossRef]
16. Wang, P.; Qiao, G.; Zhang, Y.; Hou, D.; Zhang, J.; Wang, M.; Wang, X.; Hu, X. Molecular dynamics simulation study on interfacial shear strength between calcium-silicate-hydrate and polymer fibers. *Constr. Build. Mater.* **2020**, *257*, 119557. [CrossRef]
17. Qiao, G.; Hou, D.; Wang, P.; Lu, Z. Insights on failure modes of calcium-silicate-hydrate interface strengthened by polyacrylamides: Structure, dynamic and mechanical properties. *Constr. Build. Mater.* **2021**, *278*, 122406. [CrossRef]
18. Liu, K.; Cheng, X.; Ma, Y.; Gao, X.; Zhang, C.; Li, Z.; Zhuang, J. Analysis of interfacial nanostructure and interaction mechanisms between cellulose fibres and calcium silicate hydrates using experimental and molecular dynamics simulation data. *Appl. Surf. Sci.* **2020**, *506*, 144914. [CrossRef]
19. Zhou, Y.; Tang, L.; Liu, J.; Miao, C. Interaction mechanisms between organic and inorganic phases in calcium silicate hydrates/poly (vinyl alcohol) composites. *Cem. Concr. Res.* **2019**, *125*, 105891. [CrossRef]

20. Zhou, Y.; Hou, D.; Jiang, J.; She, W.; Li, J. Molecular dynamics study of solvated aniline and ethylene glycol monomers confined in calcium silicate nanochannels: A case study of tobermorite. *Phys. Chem. Chem. Phys.* **2017**, *19*, 15145–15159. [CrossRef]
21. Duan, Y.; Zheng, H.; Wang, P.; Hou, D.; Wang, M.; Yin, B.; Li, S. Molecular dynamics simulation study on the hydrophobic mechanism of Ettringite nanoporous channels modified by silane and silane/graphene oxide. *Appl. Surf. Sci.* **2023**, *623*, 156975. [CrossRef]
22. Moore, A.; Taylor, H. Crystal structure of ettringite. *Acta Crystallogr. Sect. B Struct. Crystallogr. Cryst. Chem.* **1970**, *26*, 386–393. [CrossRef]
23. Jueshi, Q.; Jinchen, Y.; Huaqiang, S.; Ying, M. Formation and Function of Ettringite in Cement Hydrates. *J. Chin. Ceram. Soc.* **2017**, *45*, 1569–1581. [CrossRef]
24. Skoblinskaya, N.; Krasilnikov, K. Changes in crystal structure of ettringite on dehydration. 1. *Cem. Concr. Res.* **1975**, *5*, 381–393. [CrossRef]
25. Cygan, R.T.; Liang, J.-J.; Kalinichev, A.G. Molecular models of hydroxide, oxyhydroxide, and clay phases and the development of a general force field. *J. Phys. Chem. B* **2004**, *108*, 1255–1266. [CrossRef]
26. Honorio, T.; Guerra, P.; Bourdot, A. Molecular simulation of the structure and elastic properties of ettringite and monosulfoaluminate. *Cem. Concr. Res.* **2020**, *135*, 106126. [CrossRef]
27. Cannon, W.R.; Pettitt, B.M.; McCammon, J.A. Sulfate anion in water: Model structural, thermodynamic, and dynamic properties. *J. Phys. Chem.* **1994**, *98*, 6225–6230. [CrossRef]
28. Shahriyari, R.; Khosravi, A.; Ahmadzadeh, A. Nanoscale simulation of Na-Montmorillonite hydrate under basin conditions, application of CLAYFF force field in parallel GCMC. *Mol. Phys.* **2013**, *111*, 3156–3167. [CrossRef]
29. Plimpton, S.; Crozier, P.; Thompson, A. LAMMPS-large-scale atomic/molecular massively parallel simulator. *Sandia Natl. Lab.* **2007**, *18*, 43.
30. Nosé, S. A unified formulation of the constant temperature molecular dynamics methods. *J. Chem. Phys.* **1984**, *81*, 511–519. [CrossRef]
31. Keil, F. Multiscale modelling in computational heterogeneous catalysis. In *Multiscale Molecular Methods in Applied Chemistry*; Springer: Berlin/Heidelberg, Germany, 2011; pp. 69–107.
32. Evans, D.J.; Hoover, W.G.; Failor, B.H.; Moran, B.; Ladd, A.J. Nonequilibrium molecular dynamics via Gauss's principle of least constraint. *Phys. Rev. A* **1983**, *28*, 1016. [CrossRef]
33. Wang, P.; Yang, Q.; Jin, Z.; Hou, D.; Wang, M. Effects of water and ions on bonding behavior between epoxy and hydrated calcium silicate: A molecular dynamics simulation study. *J. Mater. Sci.* **2021**, *56*, 16475–16490. [CrossRef]
34. Bezerra, E.M.; Joaquim, A.P.; Savastano, H. Some properties of fiber-cement composites with selected fibers. In Proceedings of the Conferencia Brasileira de Materiais e Tecnologias Não Convencionais: Habitações e Infra-Estrutura de Interesse Social Bra-sil-NOCMAT, Pirassununga, SP, Brasil, 3 November 2004; pp. 34–43.
35. Humphrey, W.; Dalke, A.; Schulten, K. VMD: Visual molecular dynamics. *J. Mol. Graph.* **1996**, *14*, 33–38. [CrossRef] [PubMed]
36. Han, Q.; Yang, Y.; Zhang, J.; Yu, J.; Hou, D.; Dong, B.; Ma, H. Insights into the interfacial strengthening mechanism of waste rubber/cement paste using polyvinyl alcohol: Experimental and molecular dynamics study. *Cem. Concr. Compos.* **2020**, *114*, 103791. [CrossRef]
37. Taylor, H.; Famy, C.; Scrivener, K. Delayed ettringite formation. *Cem. Concr. Res.* **2001**, *31*, 683–693. [CrossRef]
38. Wang, M. *Reaserch on the Properties and Mechanism of High Performance Cement–Based Materials*; Northwestern Polytechnical University: Xi'an, China, 2018.
39. Sowoidnich, T.; Rachowski, T.; Rößler, C.; Völkel, A.; Ludwig, H.-M. Calcium complexation and cluster formation as principal modes of action of polymers used as superplasticizer in cement systems. *Cem. Concr. Res.* **2015**, *73*, 42–50. [CrossRef]
40. Zhou, Y.; Huang, J.; Yang, X.; Dong, Y.; Feng, T.; Liu, J. Enhancing the PVA fiber-matrix interface properties in ultra high performance concrete: An experimental and molecular dynamics study. *Constr. Build. Mater.* **2021**, *285*, 122862. [CrossRef]
41. Chen, B.; Qiao, G.; Hou, D.; Wang, M.; Li, Z. Cement-based material modified by in-situ polymerization: From experiments to molecular dynamics investigation. *Compos. Part B Eng.* **2020**, *194*, 108036. [CrossRef]
42. Hou, D.; Li, Z.; Zhao, T. Reactive force field simulation on polymerization and hydrolytic reactions in calcium aluminate silicate hydrate (C–A–S–H) gel: Structure, dynamics and mechanical properties. *Rsc. Adv.* **2015**, *5*, 448–461. [CrossRef]